

Online Research @ Cardiff

This is an Open Access document downloaded from ORCA, Cardiff University's institutional repository: <https://orca.cardiff.ac.uk/id/eprint/119193/>

This is the author's version of a work that was submitted to / accepted for publication.

Citation for final published version:

Sarma, Plaban Jyoti, Dey Baruah, Satyajit, Logsdail, Andrew ORCID: <https://orcid.org/0000-0002-2277-415X> and Deka, Ramesh Chandra 2019. Hydride pinning pathway in the hydrogenation of CO₂ into formic acid on dimeric tin dioxide. ChemPhysChem 20 (5) , pp. 680-686. 10.1002/cphc.201801194 file

Publishers page: <http://dx.doi.org/10.1002/cphc.201801194>
<<http://dx.doi.org/10.1002/cphc.201801194>>

Please note:

Changes made as a result of publishing processes such as copy-editing, formatting and page numbers may not be reflected in this version. For the definitive version of this publication, please refer to the published source. You are advised to consult the publisher's version if you wish to cite this paper.

This version is being made available in accordance with publisher policies.

See

<http://orca.cf.ac.uk/policies.html> for usage policies. Copyright and moral rights for publications made available in ORCA are retained by the copyright holders.



Hydride Pinning Pathway in the Hydrogenation of CO₂ into Formic Acid on Small Tin Dioxide Clusters

Plaban Jyoti Sarma,^[a] Satyajit Dey Baruah,^[a] Andrew Logsdail^[b] and Ramesh Chandra Deka^{*[a]}

Abstract: Capture of CO₂ and conversion into organic feedstocks, are of increasing need as society moves to a renewable energy economy. Here, a hydride assisted selective reduction pathway is proposed for the conversion of CO₂ to formic acid (FA) over SnO₂ monomer and dimer. Our density functional theory (DFT) calculations infer the strong chemisorption of CO₂ on SnO₂ clusters by forming a carbonate structure, whereas heterolytic cleavage of H₂ provides a new pathway for the selective reduction of CO₂ to formic acid at low overpotential. Among two investigated pathways for reduction of CO₂ to HCOOH, the hydride pinning pathway is found promising with a unique selectivity for HCOOH. The negatively-charged hydride forms on the cluster during the dissociation of H₂ and facilitates the formation of formate intermediate, which determines the selectivity for FA over alternative CO and H₂ evolution reaction. It is confirmed that SnO₂ clusters exhibit different catalytic behaviour than surface equivalents, thus offering promise for future work investigating the reduction of CO₂ to FA via a hydride pinning pathway at low overpotential and CO₂ capturing.

Introduction

CO₂ is a color- and odor-less gas that contributes significantly to the phenomenon of global warming. Consumption of fossil fuels and various anthropogenic sources has led to the ceaseless emission of CO₂ pertaining to both short and long-term threat to the mankind and all alike.^[1,2] Therefore, there has been sustained academic and commercial attempts to improve current methods of conversion or trapping of this potent greenhouse gas. Conversion of CO₂ into valuable chemicals such as HCOOH, CH₃OH, CO etc. is desirable due to their individual applications.^[3-6] Among them, reduction of CO₂ into formic acid and methanol opens the route for the storage and transportation of H₂, which itself is considered a fuel of the future. Hence, both HCOOH and MeOH can serve as potential liquid chemical hydrogen storage (CHS) materials.^[7] Additionally, HCOOH exists as a liquid at room temperature and can be used in a direct formic acid fuel cell.^[8] Apart from that, HCOOH would prove to be more beneficial compared to other organic feedstocks due to nontoxic nature as well as ease in transportability. However, the conversion process which is critical because of its thermodynamic stability (C=O bond

about the activation of CO₂.^[9] There are several possible methods by which CO₂ reduction can be performed, such as catalytic hydrogenation; complex metal hydrides, electrochemical reduction, photocatalysis and biological reduction. Among these methods, electro- and photo-chemical reduction of CO₂ to HCOOH are promising because of their high efficiency, product selectivity and lower production cost.^[10-12]

Recently, Sn-based electrodes have gained popularity as a suitable catalyst because of their low toxicity and price for large-scale application.^[13,14] Tin electrodes show relatively high overpotential resulting from the higher Tafel slope value (254 mV dec⁻¹) for the H₂ evolution reaction, a major competing reaction with the HCOOH formation, making the catalyst more selective towards the reduction of CO₂ to FA.^[15] Like other non-noble metal electrodes, Sn electrodes also undergo corrosion and degradation, which leads to the deactivation of the catalyst,^[16] but the effect tends to be good for Sn because the oxide layer is also catalytically active for the CO₂ reduction. Chen and Kanan have studied the importance of the oxide layer in the mechanism and reported that catalytic activity in presence of the oxide layer is proportional to the reduction efficiency.^[17]

Numerous experimental studies have focused on the selective CO₂ electroreduction to formic acid using tin dioxide nanoparticles.^[18-20] Meyer and co-workers investigated that by controlling nanoparticle size, a high current density of >10 mA/cm², corresponding to formate production, can be achieved at a lower overpotential of ~340 meV.^[21] In another study, Kumar et al. discussed the activity of reduced SnO₂ nanowires towards the selectivity for HCOOH.^[22] They revealed that the nanoporous nature and high numbers of grain boundaries of the particles are major factors in the enhancement of the rate and selectivity of HCOOH production. In comparison with the experimental studies theoretical investigations on the proper mechanism of CO₂ reduction to formic acid over SnO₂ catalyst are few. In the reported literature, the mechanism is initiated by the activation of CO₂, where the chemisorption of CO₂ results in a change of structure from linear to bent. After that, successive addition of 'H' to the CO₂ leads to the formation of formic acid. Moreover, the transfer of 'H' to the 'C' or 'O' of the CO₂ will determine the selectivity for the HCOOH or CO respectively.^[23] Cui et al. explained the effect of surface hydroxyls on the reduction mechanism, where they promote the formation of HCOOH as a major product.^[24] All these studies are relevant to the SnO₂ surface, but the mechanism on small sized tin dioxide, where quantum confinement and morphology are influential, remains unknown. The controlled synthesis of ~0.5-2.5 nm SnO₂ quantum dots is reported by Xu et al. and studied their catalytic behaviour towards ethanol sensing. They observed that the SnO₂ QDs shows higher sensitivity than relatively higher sized SnO₂ nanowires.^[25] In addition, SnO₂ particles are also synthesized in gas phase via detonation process where Yan and coworkers reported the lowest diameters of the particle is 1 nm.^[26] Therefore, in our current study, we aim to predict the global minimum structure of SnO₂ and Sn₂O₄ clusters and investigate their catalytic behaviour towards hydrogenation of CO₂. We identified that the growth of the nanocluster is different from the bulk and

[a] Mr. Plaban Jyoti Sarma, Mr. Satyajit Dey Baruah, Prof. Ramesh Chanda Deka
Department of Chemical Sciences
Tezpur University
Napaam, Sonitpur, Assam, India-784018
E-mail: ramesh@tezu.ernet.in
[b] Dr. Andrew Logsdail
School of Chemistry
Cardiff Catalysis Institute, Cardiff University, Cardiff CF10 3AT, UK

Supporting information for this article is given via a link at the end of the document.

energy ~533 kJ/mol), requires a suitable catalyst that can bring

hence the catalytic properties are also different from bulk and the surface.

Selective CO₂ reduction to formic acid has also been studied on other metal clusters,^[27,28] metal complexes,^[29] ionic liquids,^[30] transition metal surfaces,^[31,32] metal-hydride^[33,34] and surfaces of In₂O₃, CeO₂, ZnO etc.^[12,35-37] On the Cu-hydride nanocluster, CO₂ reduction follows a different mechanism where CO₂ get activated in the influence of lattice hydride and forms formate intermediate at an overpotential of 0.32 eV.^[38] This investigation paves a new way of thinking about the hydride assisted pathway for the selective reduction CO₂ to FA over metal oxide nanoparticles; we have built our understanding around the interaction of CO₂ and dissociation of H₂ on small SnO₂ monomer and dimer, and subsequently investigated a new and selective path for the conversion of CO₂ into formic acid.

Results and Discussion

Global minimum structures of SnO₂ and Sn₂O₄ cluster.

Structures of both SnO₂ and Sn₂O₄ clusters are optimized at MN12-SX/def2TZVPP level of theory (Figure 1). For SnO₂ cluster only a single isomer is found whereas for Sn₂O₄ we are reporting three low lying configurational isomer and they are presented in Fig. S1. Both GM structures are symmetric and fall in the 'D' group. SnO₂ cluster provides only one binding sites (Sn-O) for the guest molecule whereas the dimeric Sn₂O₄ structure offers two binding sites, the terminal 'Sn-O' and the bridging 'Sn-O' site. On the basis of the information as discussed, in the next sections we describe the adsorption of CO₂ and dissociation of H₂ on both of these clusters, followed by the reduction mechanism of CO₂.

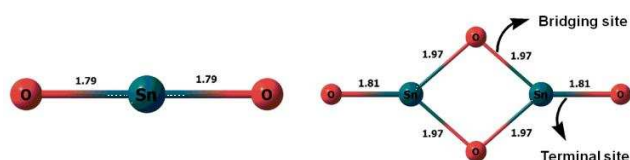


Figure 1. DFT optimized structure of SnO₂ and Sn₂O₄ cluster along with their symmetry point group and structural parameters.

Adsorption of CO₂ on SnO₂ and Sn₂O₄ clusters.

Optimized geometries illustrating the chemisorption behaviour of CO₂, on all the possible sites of both clusters, are given in Figure 2. For SnO₂, the CO₂ takes the form of carbonate structure after chemisorption, where 'O' of the CO₂ binds with the Sn-center and 'C' makes bond to 'O' of the cluster. The chemisorption on metal oxides of CO₂ has been observed to result in carbonate formation in the previous studies by Cui et al.^[24] The differences in C=O bond length and CO₂ bond angle for the transition state and chemisorbed structures also demonstrates the activation of CO₂ on the SnO₂ cluster. The characteristic Sn-O bond length changes from 1.84 Å in transition state to 1.97 Å in the chemisorbed SnO₂CO₂-C and Sn₂O₄CO₂-C_T, while in the Sn₂O₄CO₂-C_B, the parent 'Sn-O' bond dissociates and forming a new 'Sn-O' bond with the 'O' of CO₂ maintaining a bond distance of 1.96 Å. (vdWc= van der Waals complex, C=Chemisorption, T=Terminal position, B=Bridging position). At the same time, the C-O bond elongates from 1.21 Å to 1.34-1.36 Å once CO₂ is bonded to the cluster. In addition, the ∠O-C-O bond angle changes from 148°-157° in TS to the range of 121°-126° in chemisorbed clusters, which is also

satisfying the chemisorbed range for CO₂ and correlating with reported activation range of CO₂.^[24,37] From this scenario, we can clearly see that the process of CO₂ activation occurs when the dimensionality of the molecule changes from linear to a planer carbonate structure.

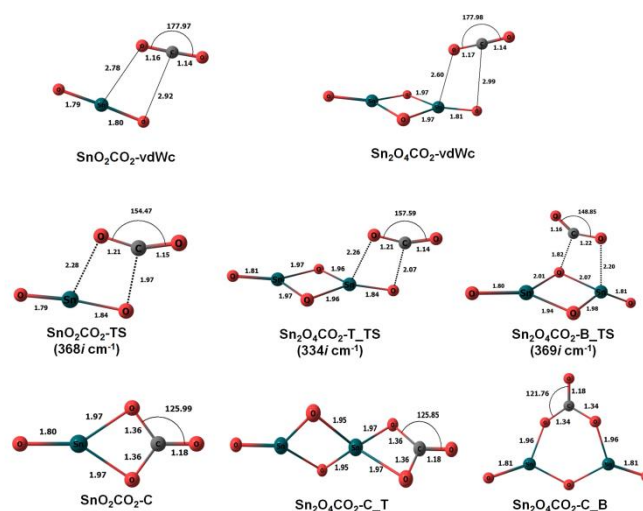


Figure 2. MN12-SX optimized structures of van der Waals complexes of CO₂ interaction as SnO₂CO₂-vdWc and Sn₂O₄CO₂-vdWc, chemisorbed CO₂ structures as SnO₂CO₂-C, Sn₂O₄CO₂-C_T and Sn₂O₄CO₂-C_B and the transition state for the interaction of CO₂ along with the bond length and bond angle. vdWc=van der Waals complex, C=Chemisorption, T=Terminal position, B=Bridging position, TS=Transition state.

Free energies of adsorption and activation energy for the adsorption of CO₂ are calculated to understand the thermodynamic feasibility of the adsorption. The adsorption energy of SnO₂CO₂-C is -0.26 eV (-5.98 kcal/mol) with an activation energy of 0.51 eV (11.84 kcal/mol), whereas, for Sn₂O₄CO₂-C_T and Sn₂O₄CO₂-C_B are -0.60 eV (-13.78 kcal/mol) and 0.64 eV (14.76 kcal/mol) respectively. The calculated barrier height values for Sn₂O₄CO₂-C_T and Sn₂O₄CO₂-C_B are found 0.39 eV (8.91 kcal/mol) and 0.90 eV (20.77 kcal/mol). These analyses reveal that in both clusters, the terminal position is the suitable site for the adsorption of CO₂ whereas the bridging site is not preferable in Sn₂O₄, as a substantial energy of 0.64 eV is required.

Dissociation of H₂ on SnO₂ and Sn₂O₄ clusters.

Like CO₂ adsorption, H₂ finds one active site on SnO₂ cluster and two (terminal 'Sn-O' and bridging 'Sn-O') sites for Sn₂O₄ cluster for dissociation. The clusters with dissociated H₂ are shown in Figure 3.

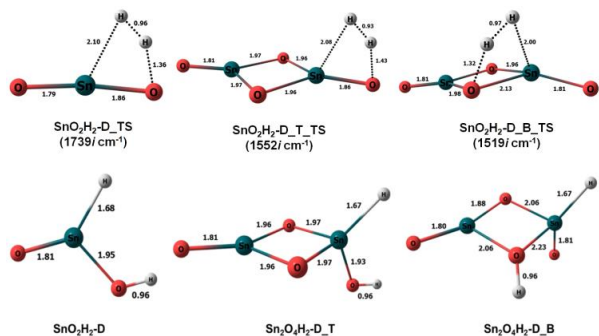


Figure 3. Optimized figures of H_2 dissociated clusters along with transition state structures at MN12-SX/def2TZVPP level of theory. (D=Dissociation, T=Terminal and B=bridging).

H_2 dissociation is thermodynamically favourable on both clusters, which is assessed from free energy of dissociation given in Table 1. Along with the dissociated cluster, we are presenting the transition state for the H_2 dissociation on both the clusters. In the monomer the barrier height is calculated 1.48 eV (34.158 kcal/mol) whereas, in dimeric cluster, two transition states are simulated to understand the dissociation nature in the terminal and bridging 'Sn-O' site. It is noteworthy to mention that although the barrier height corresponding to the H_2 dissociation in bridging 'Sn-O' site is more than in the terminal Sn-O site (table 1) but the elongation of 'H-H' bond length is more (0.97 Å) in Sn_2O_4 -D_B_TS than the other two transition states. Therefore, it can be understood that even though the kinetic barrier is little more in Sn_2O_4 -D_B_TS than Sn_2O_4 -D_T_TS but the dissociation is predominant in the bridged position. Besides, in the TS (Sn_2O_4 -D_B_TS), along with the elongation of H-H bond, the bridging 'Sn-O' bond also get elongated to 2.13 Å from 1.97 Å in the free Sn_2O_4 which is a consequence of the substantial activation energy found in Sn_2O_4 -D_B_TS. In the dissociated clusters the formed 'Sn-H' bond lengths are 1.68 Å and 1.67 Å in the SnO_2 and Sn_2O_4 cluster respectively, while, the newly formed O-H bonds are found equal in length in all dissociated sites and that is 0.96 Å. To verify the formation of hydride in each cluster, we have calculated Bader charge of each atom in the chemisorbed structure (Table 1). Bader charges of 'H' in SnO_2H_2 -D, $Sn_2O_4H_2$ -D_T and $Sn_2O_4H_2$ -D_B are -0.280, -0.276 and -0.270 e respectively, indicating a gain in electron density. At this point, it is important to describe the structures of the dissociated clusters, since; the reaction mechanism of CO_2 reduction is dependent on the position of the 'H' atoms. SnO_2H_2 -D is planar with the O-H hydrogen pointing out of the plane. In both $Sn_2O_4H_2$ -D_T and $Sn_2O_4H_2$ -D_B, the Sn-center takes a distorted tetrahedral arrangement. The analysis of $\angle O$ -Sn-H bond angles is calculated: for $Sn_2O_4H_2$ -D_T, the $\angle O$ -Sn-H angle, with respect to the bridging O atoms, is $\sim 120^\circ$, whereas in $Sn_2O_4H_2$ -D_B the angles are nearer to $\sim 100^\circ$ (Figure S2). This indicates the axial orientation of the hydride in $Sn_2O_4H_2$ -D_B. Another effect associated with the structure of $Sn_2O_4H_2$ -D_B, that after dissociation the Sn-O(H) bond length increases to 2.23 Å, as a result of which the hydride tends to orient to axial position with respect to 'Sn'. To confirm our understanding of the bonding of Sn with hydride, we have also plotted a projected density of states (PDOS) for the atoms involved in 'Sn-H' bond (Supporting Information, Figure S2). The PDOS shows stronger interaction of '5s' and '5p' orbitals of Sn with the H '1s' in $Sn_2O_4H_2$ -D_T than in $Sn_2O_4H_2$ -D_B. This assessment suggests that the Sn 5s orbitals

are involved in the bonding of 'Sn-H' in $Sn_2O_4H_2$ -D_T, as is also reflected by the larger $\angle O$ -Sn-H bond angle (typically 120° for sp^2 hybridized orbital).

Table 1. Free energy of dissociation of H_2 on SnO_2 clusters at 298 K. Also given are the Bader charges of reacting atoms on all the sites of the clusters (D=Dissociation, T=Terminal and B=bridging).

Properties	Bond types	Atoms	SnO_2H_2 -D	$Sn_2O_4H_2$ -D_T	$Sn_2O_4H_2$ -D_B
Free energy of Dissociation in eV (kcal/mol)			-1.26 (-29.15)	-2.04 (-46.98)	-0.64 (-14.85)
Activation energy eV (kcal/mol)			1.48 (34.18)	1.24 (28.79)	1.52 (35.10)
Bader charge of characteristic atoms e	(Sn-)H	Sn	1.921	2.162	2.010
		H	-0.280	-0.276	-0.270
	(O-)H	O	-1.249	-1.257	-1.340
		H	0.634	0.641	0.672

Mechanisms for CO_2 reduction

We have investigated two pathways for the reduction of CO_2 on SnO_2 clusters (Table 2):

- Case I: The formation of formic acid (FA) in a concerted process, where H_2 comes from the gas phase and dissociates on the terminal C=O bond to form FA. Both SnO_2CO_2 -C and $Sn_2O_4CO_2$ -C_T are eligible for this mechanism, as adsorption of CO_2 on both clusters is thermodynamically favourable.
- Case II (Hydride Pinning pathway): The step-wise formation of FA via a formate intermediate. Due to the presence of extra Sn-center in the Sn_2O_4 cluster, this mechanism is only considered for the Sn_2O_4 cluster: In the first step, the 'O' of CO_2 binds to a suitable Sn binding-site and simultaneously the 'C' is taking the hydride from the cluster. Then, in the second step, the remaining H is transferred to the unbound O of the adsorbed $HCOO^*$ intermediate.

Table 2. Two different Cases that are considered for the formation of HCOOH from reduction of CO_2

Pathway	Reaction
HCOOH formation via case I	$CO_2^* + H_2 \rightarrow HCOOH^*$
HCOOH formation via case II	$CO_2 + H^* \rightarrow HCOO^*$ $HCOO^* + H^* \rightarrow HCOOH$

CO_2 reduction to HCOOH on both SnO_2 and Sn_2O_4 cluster via Case I.

This mechanism is effectively the direct hydrogenation of CO_2 to Formic acid, with H_2 dissociation taking place on the unbound C=O bond of SnO_2CO_2 -C and $Sn_2O_4CO_2$ -C_T. Since the formation of HCOOH does not involve any intermediate, the whole reaction has only one transition state, represented as TS1 and TS2 in Figure 4. These TSs correspond to the formation of HCOOH on SnO_2 and Sn_2O_4 clusters and are characterized by

the presence of one imaginary frequency of 2246i cm⁻¹ and 2249i cm⁻¹.

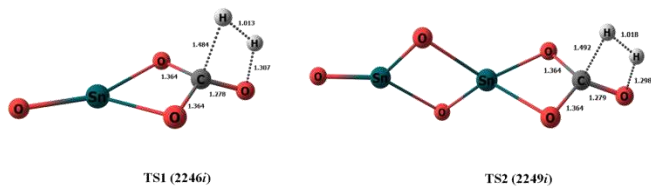


Figure 4. Transition states TS1 and TS2 for the formation of HCOOH via case I.

In the transition state, the H••H bond is elongated from 0.74 Å to 1.01 Å when adsorbed on the cluster. The bond distance of newly formed C••H bonds are 1.48 Å and 1.49 Å, whereas the O••H bonds are 1.30 Å and 1.29 Å in TS1 and TS2 respectively. The free energy profile diagram presented in Figures 5, signify the case I pathway for the CO₂ reduction on SnO₂ and Sn₂O₄ cluster respectively.

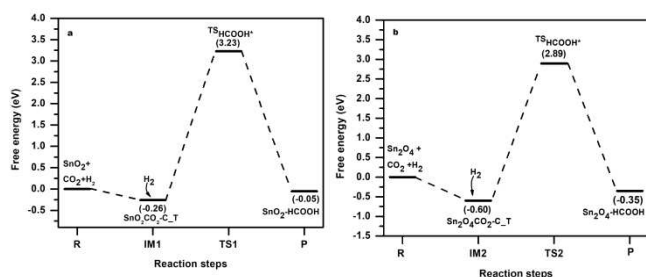


Figure 5: Free energy profile for CO₂ reduction on SnO₂ (a) and Sn₂O₄ (b) clusters via Case I, as calculated at MN12-SX/def2tzvpv level of theory.

From Figure 5, we can see that the free energies of activation for TS1 and TS2 are 3.492 eV (80.54 kcal/mol) and 3.490 eV (80.50 kcal/mol), respectively, which is substantial. The difference in energy between the TSs is only 0.002 eV, so the energetic profiles are very similar for both of the clusters towards catalytic formation of HCOOH via Case I. Clearly, the major drawback of this mechanism is the large energy barrier, which would lead to kinetic infeasibility for the reaction. The high activation energy is attributed to the strong binding of CO₂ with the clusters; additionally, for the final product, the formed HCOOH binds favourably in a tetrahedral manner with the Sn-center in the cluster, rather than leaving the catalytic site and this could deactivate the catalyst. Thus, we can conclude that CO₂ reduction is infeasible via this mechanism, though an alternative conclusion is that the strong binding of CO₂ with the cluster offers promise for application as a carbon dioxide trapping material, which is very important part of CO₂ mitigation.

CO₂ reduction to HCOOH on Sn₂O₄ cluster via Case II.

We have already mentioned while introducing the Case II that the 'Hydride pinning pathway' is only feasible for the Sn₂O₄ cluster. Thus, the first question to address is why the monomeric cluster is not a suitable candidate for this mechanism: the lack of a second Sn-center in the cluster limits HCOO formation and hence

formic acid. As a result, rather forming a formate intermediate, carbonate structure is reformed via the chemisorption of CO₂ (Figure S3). This outcome is due to the unsaturated nature of 'Sn' in SnO₂ cluster.

In the hydride pinning step over Sn₂O₄, the HCOO* intermediate forms as a result of the transfer of hydride from the Sn₂O₄ cluster to the 'C' of CO₂ and simultaneously the 'O' of CO₂ binds with another Sn-center in the cluster. Before unraveling the in-depth detailed mechanistic pathway, it is worth mentioning that, even though H₂ dissociates heterolytically on both terminal and bridging Sn-O sites of the Sn₂O₄ cluster, to give Sn₂O₄H₂-D_T and Sn₂O₄H₂-D_B, the hydride pinning pathway proceeds only via the formation of Sn₂O₄H₂-D_B. The reason for this selectivity is attributed to the hydride orientation towards the CO₂ binding site, whereas the hydride of Sn₂O₄H₂-D_T is oriented away from the CO₂ binding site. These observations strongly suggest that the mechanism proceeds via Sn₂O₄H₂-D_B, followed by the hydride pinning step.

A free energy diagram for the overall reaction mechanism is presented in Figure 6. The favorable interaction at the pinning step (IM3 → IM4') is mainly attributed to the attraction of positively charged 'C' of CO₂ towards the negatively charged hydride. In this step, CO₂ comes from the gas phase and proceed through a transition state TS3 (574i cm⁻¹) with an activation energy of 1.15 eV (26.51 kcal/mol) to take up the hydride from the 'Sn'. In TS3, the C••H and Sn••O distances are 1.48 Å and 2.26 Å, respectively, whereas the bond length that corresponds to the breaking of Sn••H bond is 1.81 Å. The formed HCOO* intermediate (IM4) remains adsorbed on the cluster via one 'O' of CO₂, with the unbound 'O' of the HCOO* oriented away from the cluster, however a spontaneous structural transformation occurs with a free energy change (ΔG) of -0.52 eV (-11.99 kcal/mol) which gives IM4' where, the 'O=C-H' group flips around the Sn-O single bond. Finally, IM4' has the (C-)H pointed upward and the unbound 'O' makes a weak stabilizing interaction with the Sn maintaining 2.38 Å of bond distance. A major advantage of this structural change is that the weakly bonded 'O' is now nearer to the second hydrogen, which is bonded to one of the bridging 'O' of the cluster. In the last step, the remaining 'H' is transferred to the 'O' and forms HCOOH via a transition state TS4 (1003i cm⁻¹), with an activation energy of 0.33 eV (7.63 kcal/mol). In the same step the HCOOH also desorbs from the catalytic site, thus facilitating the regeneration of the catalyst to undergo H₂ dissociation and repeat the catalytic cycle.

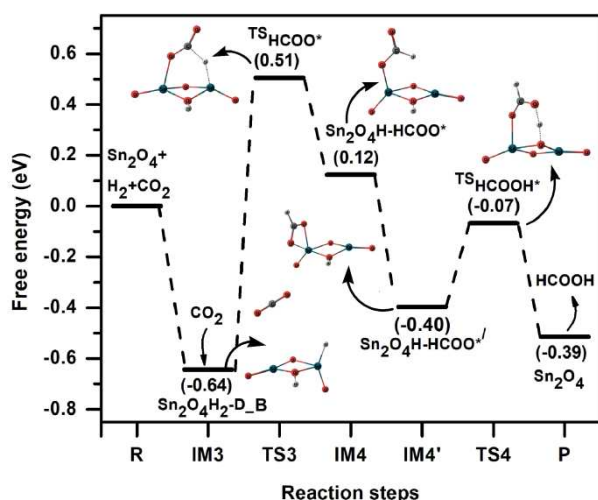


Figure 6. Complete potential energy surface diagram for hydride pinning pathway (Case II) for CO_2 reduction calculated at MN12-SX/def2tzvpp level of theory.

After analysis of the free energy diagram, we can clearly state that the pinning step (hydride transfer) is the rate determining step (RDS) of the reaction. Moreover, in this RDS, the ΔG difference between the IM3 and IM4' is only 0.24 eV, which is an indicator of the necessary overpotential for HCOOH production vs RHE. Previous experimental studies report the overpotential for HCOOH formation on SnO_2 nanoparticles as 0.34-0.35 eV^[21,22] and theoretical value reported on copper hydride ($\text{Cu}_{32}\text{H}_{20}\text{L}_{12}$, $\text{L}=\text{S}_2\text{PH}_2$) nanocluster is 0.32 eV.^[38] The simulation models and experimental catalysts differ in size but the consistency between results confirms the validity of our approach; furthermore, the subtle differences between experimental and calculated overpotential suggest opportunities to tune the size of the nanoparticle specifically to aid the reduction mechanism of CO_2 to formic acid. The overall reaction cycle for the hydride pinning pathway is shown in Figure 7.

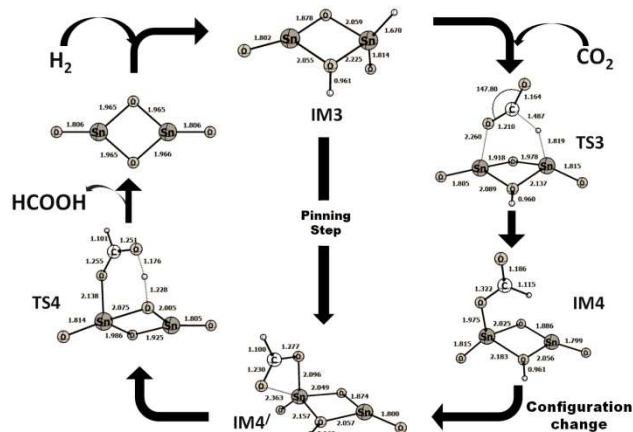


Figure 7. Total reaction Cycle of HCOOH formation from CO_2 via hydride pinning pathway.

Thus far, we have discussed the formation of formic acid via the hydride mechanism, but there exist other competing processes such as H_2 evolution reaction and CO formation reactions along with the HCOOH formation. To consider these side reactions, we have studied the H_2 recombination reaction using the $\text{Sn}_2\text{O}_4\text{H}_2\text{-D}_\text{B}$ structure as a source for H_2 evolution. The ΔG^\ddagger and ΔG for the H_2 recombination reaction are found to be 2.17 eV and 0.64 eV, respectively. A free energy diagram, shown in Figure S4 is the comparison between the formate formation and H_2 recombination reactions, alongside the structure of transition state corresponding to the H_2 recombination. Therefore, H_2 recombination will not hinder the HCOOH formation. On the other hand, formation of CO along with H_2O will be inevitable if the hydride is transferred to the 'O' of CO_2 instead of 'C'. We have substantiated two factors to describe the inhibition of CO formation: 1) the hydride lacks adequate ability to bond with the 'O' of CO_2 as both are negatively charged i.e. coulombic repulsion; 2) there is an absence of a binding site for a COOH intermediate. To confirm this, we have modelled a structure where 'O' of CO_2 takes the 'H' from 'Sn' and forms COOH* intermediate (SI, Figure S5). We have demonstrated that, after formation of a COOH* intermediate, reorientation is necessary with adsorption to the cluster via the 'C' atom. This is also observed in previous literature by Tang et al.^[38] but the bridging oxygens of our cluster are coordinately saturated, so a carbonate structure will be formed if 'C' binds to the terminal 'O' of the cluster, rather picking up the 'H' from the Sn-center to form the COOH intermediate.

Conclusions

In summary, structures and catalytic activity of SnO_2 atomic clusters are investigated towards the reduction of CO_2 using DFT method. Adsorption of CO_2 on the clusters results in a stable carbonate structure whereas dissociation of H_2 opens a hydride assisted channel for reduction of CO_2 to HCOOH. The stepwise hydride pinning pathway (Case II) is auspicious in determining the selectivity for HCOOH over case I. After the formation of HCOOH, desorption of the product occurs spontaneously and the catalyst active site is regenerated. Using the computational hydrogen

electrode (CHE) model, our results suggest the required overpotential for HCOOH formation is 0.24 eV. The low overpotential is a consequence of having extra Sn-center in the dimer, which plays a crucial role in stabilizing the HCOO* intermediate. Along with the HCOOH formation, H₂ recombination is also studied and a large activation barrier of 2.12 eV confirms that H₂ evolution is not a major issue in the hydride pinning mechanism. Moreover, the presence of hydride in the cluster inhibits the formation of COOH* intermediate and therefore, CO formation reaction is not a topic of concern in CO₂ reduction via hydride assisted pathway, as justified via coordination and electrostatic arguments. In the final touch, we put forward two benefits of using SnO₂ nanoclusters: firstly, both clusters are notable at CO₂ trapping material and, secondly, the Sn₂O₄ cluster serves as a tremendous catalyst with respect to reducing CO₂ to formic acid via the mechanism initiated by H₂ dissociation. These results offer a great platform for further experimental studies to develop our understanding of CO₂ reduction to formic acid via hydride pinning pathway.

Computational Details

Structures, reaction energies and the detailed mechanism of CO₂ reduction are studied using Kohn-Sham density functional theory (DFT) as available on Gaussian 09 quantum chemistry software package.^[39] Critical bond dissociation enthalpies of Sn-O, C-O, O-H, C-H, and Sn-H bonds are calculated at 22 tested methods employing density fitting triple- ξ def2TZVPP basis set^[40,41] as shown in Table S1. The best outcome of the initial analysis is the range-separated hybrid meta-NGA (non-separable gradient approximation) MN12-SX functional^[42] in describing bond dissociation enthalpies of the bonds close to experimental data. The accuracy of MN12-SX functional agrees with previous studies in predicting both structures and energies.^[43,44] Along with it, the def2TZVPP basis set proves very good in minimizing the basis set superposition error (BSSE), giving errors of < 0.04 eV, thus providing results close to the DFT basis set limit.^[41] Therefore, for geometry relaxation and frequency calculation, we have used MN12-SX/def2TZVPP level employing ultrafine integration grid. All reported adsorption and dissociation energies in the manuscript are also corrected appropriately for BSSE. Genetic algorithm is used for global optimization of SnO₂ and Sn₂O₄ clusters.^[45] Presence of only one imaginary frequency in the vibrational spectra confirms identified transition states, consistent with the eigenvector along the reaction coordinate, whereas, for the reactant, intermediates, and products, no imaginary frequency is observed, confirming that they are true minima. Gibbs free energy change (ΔG), at 1 atm pressure and 298K temperature are calculated for each step in the reaction mechanisms by referring to the free energy difference between the final and initial states; the calculations for the free energy of adsorption and dissociation at room temperature have been analyzed in a similar manner. The free energy of activation (ΔG^\ddagger) of the transition states are calculated by measuring the free energy change of transition state with respect to the initial state. To gain a more detailed insight into the electronic charge distribution, Bader charge analysis is done using AIMALL software package, verifying the formation of hydride on the H₂ dissociation step.^[46] As the product (HCOOH) is formed in liquid phase, a correction to the free energy for HCOOH is included in calculating the reaction

energetics, as shown in Supporting Information (Section 1). The computational hydrogen electrode (CHE) model is used to correlate the reaction free energy change with the electrochemical potential, with respect to the transfer of hydrogen from the catalyst to CO₂ while forming the HCOO* intermediate. At 1 atm, the CHE assumes that the protons and electrons are at equilibrium with the gas phase hydrogen ($H^+ + e^- \rightarrow 1/2H_2$) at potential 0V vs RHE for all pH and all temperature.^[47]

Acknowledgements

The authors are thankful to Science & Engineering Research Board (SERB) (EMR/2016/003195), Department of Science and Technology (DST) (No: DST/INSPIRE Fellowship/IF160658J) New Delhi, India, and Tezpur university for financial support. Authors acknowledge UK-India Education and Research Initiative (UKIERI) for research fund (Grant No. DST/INT/UK/P-35/2012) to carry out collaborative research work. The authors gratefully acknowledge the support of Prof. C. R. A. Catlow, FRS.

Keywords: SnO₂ and Sn₂O₄ cluster, MN12-SX Functional, CO₂ reduction, Formic acid, Hydride Pinning Pathway.

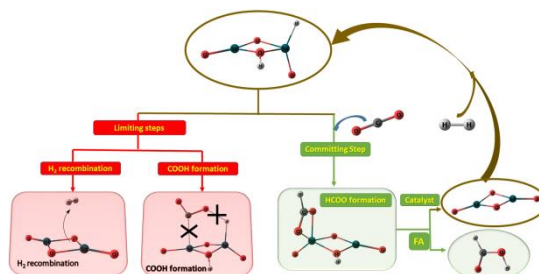
- [1] A. Stips, D. Macias, C. Coughlan, E. Garcia-Goriz, X. S. Liang, *Sci. Rep.* **2016**, *6*, 21691–21699.
- [2] J. Klankermayer, S. Wesselbaum, K. Beydoun, W. Leitner, *Angew. Chemie - Int. Ed.* **2016**, *55*, 7296–7343.
- [3] S. Roy, B. Sharma, J. Pécaut, P. Simon, M. Fontecave, P. D. Tran, E. Derat, V. Artero, *J. Am. Chem. Soc.* **2017**, *139*, 3685–3696.
- [4] A. Álvarez, A. Bansode, A. Urakawa, A. V. Bavykina, T. A. Wezendonk, M. Makkee, J. Gascon, F. Kapteijn, *Chem. Rev.* **2017**, *117*, 9804–9838.
- [5] Q. Li, J. Fu, W. Zhu, Z. Chen, B. Shen, L. Wu, Z. Xi, T. Wang, G. Lu, J. Zhu, S. Sun, *J. Am. Chem. Soc.* **2017**, *139*, 4290–4293.
- [6] D. Ballivet-Tkatchenko, S. Chambrey, R. Keiski, R. Ligabue, L. Plasseraud, P. Richard, H. Turunen, *Catalysis Today*, **2006**, *115*, 80–87.
- [7] K. Sordakis, C. Tang, L. K. Vogt, H. Junge, P. J. Dyson, M. Beller, G. Laurenczy, *Chem. Rev.* **2018**, *118*, 372–433.
- [8] X. Yu, P. G. Pickup, *Journal of Power Sources*. **2008**, *182*, 124–132.
- [9] A. Bhowmik, T. Vegge, H. A. Hansen, *Chem. Sus. Chem.* **2016**, *9*, 3230–3243.
- [10] J. Wu, Y. Huang, W. Ye, Y. Li, *Adv. Sci.* **2017**, *4*, 1–29.
- [11] A. C. Khezri, M. Fisher, J. Pumera, *Mater. Chem. A* **2017**, *5*, 8230–8246.
- [12] Y. Tamaki, K. Koike, O. Ishitani, *Chem. Sci.* **2015**, *6*, 7213–7221.
- [13] J. Wu, F. G. Risalvato, S. Ma, X. D. Zhou, *J. Mater. Chem. A* **2014**, *2*, 1647–1651.
- [14] J. Medina-Ramos, R. C. Pupillo, T. P. Keane, J. L. Dimeglio, J. Rosenthal, *J. Am. Chem. Soc.* **2015**, *137*, 5021–5027.
- [15] E. Irtam, T. Andreu, A. Parra, M. D. Hernández-Alonso, S. García-Rodríguez, J. M. Riesco-García, G. Penelas-Pérez, J. R. Morante, *J. Mater. Chem. A* **2016**, *4*, 13582–13588.
- [16] G. S. Frankel, A. Agarwal, N. Sridhar, *Electrochim. Acta* **2014**, *133*, 188–196.
- [17] Y. Chen, M. W. Kanan, *J. Am. Chem. Soc.* **2012**, *134*, 1986–1989.
- [18] S. Lee, J. D. Ocon, Y. Son, J. Lee, *J. Phys. Chem. C* **2015**, *119*, 4884–4890.
- [19] W. Lee, N. H. Cho, K. D. Yang, K. T. Nam, *Chem. Electro. Chem.* **2017**, *4*, 2130–2136.
- [20] K. R. Rao, S. Pishgar, J. Strain, B. Kumar, V. Atla, S. Kumari, J. M. Spurgeon, *J. Mater. Chem. A* **2018**, *6*, 1736–1742.
- [21] S. Zhang, P. Kang, T. J. Meyer, *J. Am. Chem. Soc.* **2014**, *136*, 1734–1737.

- [22] B. Kumar, V. Atla, J. P. Brian, S. Kumari, T. Q. Nguyen, M. Sunkara, J. M. Spurgeon, *Angew. Chemie - Int. Ed.* **2017**, *56*, 3645–3649.
- [23] K. Saravanan, Y. Basdogan, J. Dean, J. A. Keith, *J. Mater. Chem. A* **2017**, *5*, 11756–11763.
- [24] Cui, J. Han, X. Zhu, X. Liu, H. Wang, D. Mei, Q. Ge, *J. Catal.* **2016**, *343*, 257–265.
- [25] X. Xu, J. Zhuang, X. Wang, *J. Am. Chem. Soc.* **2008**, *130*, 12527–12535.
- [26] Y. Honghao, W. Linsong, L. Xiaojie, W. Xiaohong, *Rare Metal Mat. Eng.* **2013**, *42*, 1325–1327.
- [27] Cai, D. Gao, H. Zhou, G. Wang, T. He, H. Gong, S. Miao, F. Yang, J. Wang and X. Bao, *Chem. Sci.*, **2017**, *8*, 2569–2573.
- [28] C. Liu, H. He, P. Zapol, L. A. Curtiss, *Phys. Chem. Chem. Phys.* **2014**, *16*, 26584–26599.
- [29] T. N. Huan, P. Simon, A. Benayad, L. Guetaz, V. Artero, M. Fontecave, *Chem. Eur. J.* **2016**, *22*, 14029 – 14035.
- [30] T. N. Huan, P. Simon, G. Rousse, I. Genois, V. Artero, M. Fontecave, *Chem. Sci.* **2017**, *8*, 742–747.
- [31] W. Lin, K. M. Stocker, G. C. Schatz, *J. Am. Chem. Soc.* **2017**, *139*, 4663–4666.
- [32] C. Liu, T. R. Cundari, A. K. Wilson, *J. Phys. Chem. C* **2012**, *116*, 5681–5688.
- [33] W. Sun, C. Qian, L. He, K. K. Ghuman, A. P. Y. Wong, J. Jia, A. A. Jelle, P. G. O'Brien, L. M. Reyes, T. E. Wood, A. S. Helmy, C. A. Mims, C. V. Singh, G. A. Ozin, *Nat. Commun.* **2016**, *7*, 12553–12561.
- [34] K. M. Waldie, A. L. Ostericher, M. H. Reineke, A. F. Sasayama, C. P. Kubiak, *ACS Catal.* **2018**, *8*, 1313–1324.
- [35] D. Gao, Y. Zhang, Z. Zhou, F. Cai, X. Zhao, W. Huang, Y. Li, J. Zhu, P. Liu, F. Yang, G. Wang, X. Bao *J. Am. Chem. Soc.* **2017**, *139*, 5652–5655.
- [36] X. Zhao, X. Huang, X. Wang, J. Wang, *Mater. Chem. A* **2017**, *5*, 21625–21649.
- [37] X. Lu, W. Wang, S. Wei, C. Guo, Y. Shao, M. Zhang, Z. Deng, H. Zhu, W. Guo, *RSC Adv.* **2015**, *5*, 97528–97535.
- [38] Q. Tang, Y. Lee, D. Y. Li, W. Choi, C. W. Liu, D. Lee, D. E. Jiang, *J. Am. Chem. Soc.* **2017**, *139*, 9728–9736.
- [39] M. J. Frisch, G. W. Trucks, H. B. Schlegel, G. E. Scuseria, M. A. Robb, J. R. Cheeseman, G. Scalmani, V. Barone, B. Mennucci, G. A. Petersson, H. Nakatsuji, M. Caricato, X. Li, H. P. Hratchian, A. F. Izmaylov, J. Bloino, G. Zheng, J. L. Sonnenberg, M. Hada, M. Ehara, K. Toyota, R. Fukuda, J. Hasegawa, M. Ishida, T. Nakajima, Y. Honda, O. Kitao, H. Nakai, T. Vreven, J. A. Montgomery, Jr., J. E. Peralta, F. Ogliaro, M. Bearpark, J. J. Heyd, E. Brothers, K. N. Kudin, V. N. Staroverov, R. Kobayashi, J. Normand, K. Raghavachari, A. Rendell, J. C. Burant, S. S. Iyengar, J. Tomasi, M. Cossi, N. Rega, J. M. Millam, M. Klene, J. E. Knox, J. B. Cross, V. Bakken, C. Adamo, J. Jaramillo, R. Gomperts, R. E. Stratmann, O. Yazyev, A. J. Austin, R. Cammi, C. Pomelli, J. W. Ochterski, R. L. Martin, K. Morokuma, V. G. Zakrzewski, G. A. Voth, P. Salvador, J. J. Dannenberg, S. Dapprich, A. D. Daniels, Ö. Farkas, J. B. Foresman, J. V. Ortiz, J. Cioslowski, and D. J. Fox, Gaussian09 Revision D.01, Gaussian Inc. Wallingford CT. **2010**.
- [40] F. Weigend, *Phys. Chem. Chem. Phys.* **2006**, *8*, 1057–1065.
- [41] F. Weigend, R. Ahlrichs, *Phys. Chem. Chem. Phys.* **2005**, *7*, 3297–3305.
- [42] R. Peverati, D. G. Truhlar, *Phys. Chem. Chem. Phys.* **2012**, *14*, 16187–16191.
- [43] J. Frau, D. Glossman-Mitnik, *Theor. Chem. Acc.* **2018**, *137*, 67–76.
- [44] S. Paranthaman, J. Moon, J. Kim, D. E. Kim, T. K. Kim, *J. Phys. Chem. A* **2016**, *120*, 2128–2134.
- [45] M. R. Farrow, Y. Chow, S. M. Woodley, *Phys. Chem. Chem. Phys.* **2014**, *16*, 21119–21134.
- [46] AIMAll (Version 17.11.14), Todd A. Keith, TK Gristmill Software, Overland Park KS, USA, **2017** (aim.tk.gristmill.com).
- [47] J. K. Nørskov, J. Rossmeisl, A. Logadottir, L. Lindqvist, J. R. Kitchin, T. Bligaard, H. Jónsson, *J. Phys. Chem. B* **2004**, *108*, 17886–17892.

FULL PAPER

Text for Table of Contents

Representation of different paths involved in the hydrogenation of CO₂ to formic acid: The modelled Sn₂O₄ cluster has shown a unique selectivity towards HCOOH when the mechanism proceeds via hydride assisted pathway (committing step) over CO formation and H₂ recombination reactions (limiting steps).



Plaban Jyoti Sarma, Satyajit Dey Baruah, Andrew Logsdail, Ramesh Chandra Deka*

Page No. – Page No.

Hydride Pinning Pathway in the Hydrogenation of CO₂ into Formic Acid on Small Tin Dioxide Clusters